THE ASTROPHYSICAL JOURNAL, 407:219–231, 1993 April 10

THE EXCESS INFRARED EMISSION OF HERBIG Ae/Be STARS: DISKS OR ENVELOPES?

LEE HARTMANN[1] AND SCOTT J. KENYON[1]
Harvard-Smithsonian Center for Astrophysics, 60 Garden Street, Cambridge, MA 02138
AND
NURIA CALVET[2]
Centro de Investigaciones de Astronomia, Ap. Postal 264, Mérida 5101-A, Venezuela
Received 1992 July 6; accepted 1992 October 8

ABSTRACT

We suggest that the near-infrared emission of many Herbig Ae/Be stars arises in surrounding dusty envelopes, rather than circumstellar disks. Hillenbrand et al. and Lada & Adams showed that circumstellar disk models which reproduce the ~ 3 μm peaks in the near-infrared spectral energy distributions of Ae/Be stars must have high accretion rates, and must either be transparent in their inner regions, or have physical inner disk "holes." However, we show that disks around Ae/Be stars are likely to remain optically thick at the required accretion rates. Alternatively, the assumption of a physical hole in the disk implies either that large amounts of material pile up at ~ 10 stellar radii or that $\sim 90\%$ of the accretion luminosity escapes detection. To avoid these difficulties we propose that the infrared excesses of many Ae/Be stars originate in surrounding dust nebulae instead of circumstellar disks. These dust envelopes could be associated with the primary star or a nearby companion star. One picture supposes that the near-infrared emission of the envelope is enhanced by the same processes that produce anomalously strong continuum emission at temperatures ~ 1000 K in reflection nebulae surrounding hot stars. This near-infrared emission could be due to small grains transiently heated by ultraviolet photons. Some Ae/Be stars show evidence for the 3.3–3.6 μm emission features seen in reflection nebulae around hot stars, which lends further support to this suggestion. Given the difficulties of applying circumstellar disk models to Ae/Be stars, dusty nebula hypotheses deserve further consideration.

Subject headings: accretion, accretion disks — circumstellar matter — stars: emission-line, Be — stars: pre–main-sequence

1. INTRODUCTION

The Herbig Ae/Be stars are thought to be young, pre–main-sequence stars of intermediate mass (Herbig 1960; Strom et al. 1972; Finkenzeller & Jankovics 1984; Finkenzeller & Mundt 1984). Recently, Hillenbrand et al. (1992, hereafter HSVK) and Lada & Adams (1992, hereafter LA) have interpreted the excess infrared emission of these young stars with circumstellar disk models similar to those that have successfully reproduced infrared excesses of the lower mass, pre–main-sequence T Tauri stars (Adams, Lada, & Shu 1987; Kenyon & Hartmann 1987; Bertout, Basri, & Bouvier 1988). The HSVK and LA studies address the important question of whether intermediate-mass stars accrete substantial amounts of material from circumstellar disks.

One striking feature of many Ae/Be star spectral energy distributions is a local peak in the infrared excess at a wavelength of ~ 3 μm. Both HSVK and LA attribute this emission to dusty disk material heated to temperatures of ~ 2000 K. In their picture, grains evaporate at temperatures exceeding ~ 2000 K, so optically thin disk material inside the "dust destruction radius" emits less radiation than optically thick, dusty material at larger disk radii. The lack of (blackbody) emission from inner disk regions causes model spectral energy distributions of disks to decline shortward of $\lambda \sim 3$ μm; these models reproduce broadband 0.5–10 μm photometry if the dust destruction radius occurs at 5–20 stellar radii and the mass accretion through the disk exceeds $\sim 10^{-6}\ M_\odot\ \mathrm{yr}^{-1}$ (HSVK; LA).

While this interpretation for the 3 μm peak is attractive, stndard disk models do not naturally produce inner "holes" (as mentioned briefly by HSVK). As we show in this paper, the inner disks of Ae/Be stars likely remain optically thick at the high accretion rates needed to account for the observations. Small disk optical depths are possible for low accretion rates, but slow accretion does not produce obvious 3 μm peaks in the spectral energy distributions no matter how large the optically thin "hole" becomes.

As an alternative to dust destruction, HSVK suggest that inner disk holes might be caused by a stellar magnetosphere, which holds off the disk far from the stellar surface (e.g., Königl 1991). However, this model also presents difficulties, because the magnetospheric radius—and hence the maximum disk temperature—should vary considerably unless all young stars have the same magnetic field strength. More important, the total accretion luminosity must greatly exceed that indicated by the infrared, optical, and ultraviolet spectral energy distributions unless material piles up in the disk (see § 3.3.).

Mindful of these difficulties, we suggest that surrounding dusty nebulae might be the source of the 3 μm emission of many Ae/Be stars. A dusty envelope in radiative equilibrium around either the primary star or a possible companion could explain the observations with appropriate parameters; however, the envelope must lie close to the star, and should be infalling, so the missing accretion luminosity problem remains. We propose that small dust grains—transiently heated to temperatures of ~ 1000 K by ~ 10 eV photons—produce the 3 μm

[1] Visiting Astronomer, Kitt Peak National Observatory, operated by the National Optical Astronomy Observatory under contract to the National Science Foundation.
[2] Also Grup d:Astrofisica de la Societat Catalana de Fisica, Institut d'Estudis Catalans.

excess. Sellgren (1984; see also Sellgren et al. 1985) originally advanced this explanation for the 1000 K continuum and line emission from large reflection nebulae around several hot stars.

The dust envelope hypothesis seems especially applicable to the Herbig Ae/Be stars, because prominent reflection nebulae are a defining feature of the class and many Ae/Be stars clearly display significant 10–100 μm emission from an extended source (HSVK). It also accounts for the apparent lack of 3 μm emission peaks in the spectral energy distributions of F-type pre–main-sequence stars, because these stars do not emit enough $h\nu \sim 10$ eV photons to heat a large population of small grains to 1000 K. If this explanation is correct, then simple radiative equilibrium calculations are insufficient for modeling the near-infrared emission of Ae/Be stars.

We discuss the spectral energy distributions of Ae/Be stars in § 2, adding to the results of HSVK and LA by considering infrared emission features in more detail and by including ultraviolet data. Section 3 presents disk model calculations. We discuss dusty envelope models for the Ae/Be stars in § 4 and summarize our results in § 5.

2. SPECTRAL ENERGY DISTRIBUTIONS

2.1. *General Comments*

One major problem in understanding Ae/Be stars is the heterogeneity of the class, which ranges from F0 to B0 ($T_{\rm eff} \sim$ 7000–30,000 K) in spectral type and from $\sim 50\,L_\odot$ to $\gtrsim 10^5\,L_\odot$ in bolometric luminosity. Although Herbig's original definition required the presence of an A-type (or earlier) absorption spectrum, many Ae/Be stars display mainly H I and He I *emission* lines that sometimes show blueshifted P Cygni absorption components. The low-mass T Tauri stars clearly illustrate the danger of assigning spectral types solely from emission lines, because many also exhibit H I and He I emission lines and hot ($\sim$8000 K) continuous emission in addition to a late-type absorption spectrum (see Bertout et al. 1988; Basri & Bertout 1989; Hartigan et al. 1990). In fact, the optical spectra of some low-luminosity Ae/Be stars—such as R CrA (HSVK)—closely resemble the "strong emission" T Tauri stars (e.g., Cohen & Kuhl 1979), in which the underlying late-type stellar continuum cannot be seen above the hot excess emission.

Even strong absorption lines do not guarantee a reliable spectral type. For example, effective temperature estimates often rely on the strength of He I λ5876, which may be formed in the wind rather than in the stellar photosphere. This behavior clearly occurs in MWC 1080 (Fig. 1), where He I absorption is blueshifted. (Finkenzeller & Mundt's [1984] high-resolution spectrum of MWC 1080 shows no evidence for any He I absorption.) High-resolution spectra of other Ae/Be stars with complicated spectra should be acquired to investigate the He I and other features used for spectral classification (e.g., Hamann & Persson 1992b, c).

The uncertain system luminosity presents another major difficulty in understanding the spectral energy distributions of Ae/Be stars. These stars emit most of their radiation between 1000–3000 Å, so a typical extinction of $A_V \sim$ 1–2 mag results in a factor of 10–100 correction to the observed stellar luminosity. Large extinction corrections do not affect assessments of the near-infrared slope (LA) or the significance of the 3 μm peak (HSVK), but the ratio of the infrared excess luminsoity, $L_{\rm IR}$, to the stellar luminosity, L_*, does determine whether disk emission requires additional accretion energy (for large $L_{\rm IR}/L_*$) or can be powered by reprocessed starlight (for small $L_{\rm IR}/L_*$).

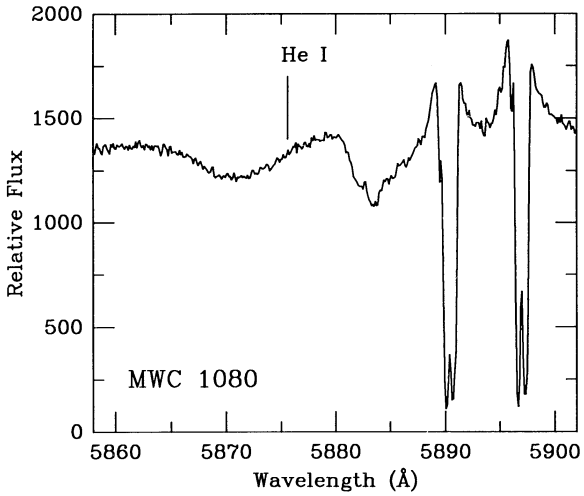

FIG. 1.—He I λ5876 and Na I resonance line absorption in the Ae/Be star MWC 1080. The He I absorption is blueshifted from the local interstellar value and extends to more than -300 km s^{-1} from line center. This spectrum was taken on 1988 December 1 with the echelle spectrograph and TI 3 CCD on the KPNO 4 m telescope, with $\sim$12 km s^{-1} resolution. Further details of the observations can be found in Hartigan et al. (1989).

All these complications limit our analysis in this paper to Ae/Be stars with reliable spectral types and infrared excesses *smaller* than the optical-ultraviolet (stellar) luminosity (HSVK's "Group I" objects). HSVK defined Group II objects to be Ae/Be stars with IR excesses flat or rising between 2 and 10 μm: for many of these objects, the infrared excess is *larger* than the apparent luminosity of the central star. HSVK point out that extensive dusty nebulae probably surround most Group II objects and that scattered light produces most of the observed optical-ultraviolet emission (see also Hamann & Persson 1992a). HSVK support this hypothesis by showing that many of these objects apear to be *below* the zero-age main sequence and have high-polarization. We cannot correct the scattered optial-ultraviolet flux to recover the total stellar luminosity, and separating possible emission from dusty envelopes and disks is difficult, so we do not consider these objects further. However, the Group II objects do constitute $\sim$25% of the Ae/Be star sample (HSVK), which will become important later in our discussion.

2.2. *Spectral Energy Distributions of Ae/Be Stars*

Guided by The Catalog of Infrared Observations (Gezari, Schmitz, & Mead 1987), we collected historical infrared observations of Ae/Be stars. We restricted our compilation to "standard" filters—J (1.25 μm), H (1.65 μm), K (2.22 μm), L (3.5 μm), M (4.8 μm), [8.4], N (10 μm), [11.1], and Q (20 μm)—and averaged the data to produce mean K magnitudes and colors ($J-K$, $H-K$, etc) for the entire sample. The central wavelengths of the broad-band filters vary by a small amount from one observatory to the next (see Bessell & Brett 1988), but we compiled these measurements at a single wavelength for simplicity. This procedure is most questionable for the 3.5 μm window, where the central wavelength varies from 3.45 μm (L) to 3.8 μm (L'; Sinton & Tittemore 1984). However, the average $K-L$ color for Ae/Be stars in our sample differs little from the average $K-L'$ color when several measurements are available, and the dispersion in $K-L$ or $K-L'$ for a single Ae/Be star is small compared to the range in $K-L$ for the entire sample.

Our infrared colors have a typical dispersion ~ 0.1 mag for a single object, and differ little from HSVK's individual measurements.

We supplemented the infrared observations with optical photometry from Herbst, Holtzman, & Phelps (1982) and Herbst, Holtzmann, & Klasky (1983), Herbig & Bell (1988, and references therein), and HSVK. As with the infrared data, we averaged multiple observations to produce a mean V brightness and optical colors ($U-V$, $B-V$, etc.). We then dereddened the combined optical and infrared data using the average $B-V$ color and the spectral type (Herbig & Bell 1988).

Finally, we assembled ultraviolet observations for a handful of Ae/Be stars—BD +61°154, AB Aur, T Ori, UX Ori, BN Ori, CO Ori, V380 Ori, BF Ori, HD 20775, HD 250550, HD 259431, CU Cha, BD +40°4124, BD +65°1637, and BD +46°3471—observed with the *International Ultraviolet Explorer* (*IUE*). We calibrated these spectra using standard methods (Harris & Sonneborn 1987), extracted average fluxes in 30 Å bandpasses centered at 0.13, 0.17, 0.22, and 0.27 μm, and dereddened these fluxes using a standard interstellar extinction curve (Savage & Mathis 1979). Although *IUE* fluxes have intrinsic accuracies of $\sim 10\%$, the biggest uncertainties in the ultraviolet spectral energy distributions arise from the extinction corrections, which can exceed 5 mag at 0.13 μm for $A_V \sim 2$ mag.

Figures 2*a*–2*c* present dereddened spectral energy distributions for 18 objects chosen to exhibit the general range of behavior and to illustrate many points made by HSVK. The spectral energy distributions often show a peak at 2–3 μm. This peak is quite pronounced in many objects (LkHα 234, RR Tau, V380 Ori, and T Ori), but is relatively small (AB Aur, UX Ori, V586 Sco or absent (HD 259431, HD 250550, HD 200775, HD 245185, CU Cha) in many others. (Our averaged photometry for HD 250550 differs from that of HSVK, who found a more pronounced 3 μm peak). In particular, roughly one-third of the Group I objects from HSVK show little or no evidence for a peak at 3 μm; moreover, the F-type members of the Ae/Be class exhibit a negligible 3 μm peak (Fig. 2*c*).

In addition to the 2–3 μm continuum excess, some Ae/Be stars display emission features in the wavelength ranges 3.3–3.6 μm and 6–11 μm similar to those observed in reflection nebulae (see § 4). In particular, CU Cha (HD 97048), XY Per, and HD 245185 exhibit 3 μm emission features in moderate-resolution spectra (Whittet et al. 1983; Brooke & Tokunaga 1992). CU Cha and Elias 1 also show emission bands throughout the 6–12 μm region at medium resolution (see Schutte et al. 1990).

Despite the large ultraviolet extinction corrections and weak ultraviolet fluxes, the 0.1–0.7 μm observations of Ae/Be stars often agree quite well with observed spectral energy distributions of normal main-sequence stars (see also Catala 1989). We find in general that using standard extinction corrections produces dereddened energy distributions that match standard A–B stars fairly well. The large R_V curve listed by Mathis (1990) for dark cloud regions tends to produce much flatter ultraviolet spectral energy distributions and, for example, provides noticeably poorer results for HD 200775 than the standard extinction curve. Some apparent mismatches are probably caused by either imprecise spectral types (e.g., HD 250550) or large photometric variability (e.g., UX Ori). The available data thus demonstrate that Ae/Be stars do not display large ultraviolet excesses over standard stars with similar spectral types.

3. DISK MODELS

3.1. *Blackbody Disk Models*

Figure 3 shows spectral energy distributions for simple optically thick blackbody disks surrounding an A0 star with a bolometric luminosity of 50 $L_\odot$ (see Kenyon & Hartmann 1990 for details concerning these calculations). The models have been calculated for both flat and "flared" disks with and without inner holes and assume a disk inclination of 0°; the height of the photosphere above the disk midplane, h, is zero everywhere for flat disks and increases with radius as $h/R = 0.1\,(R/R_*)^{1/8}$ for a flared disk (see Kenyon & Hartmann 1987), where R_* is the stellar radius. The upward curvature of the flared disk photosphere allows it to intercept more optical light from the central star at large radial distances; the disk then reemits this energy at longer wavelengths, which increases the mid- to far-infrared emission relative to that produced by a flat disk.

HSVK and LA showed that geometrically thin disks cannot reproduce the observed spectral energy distribution if these disks remain optically thick at radial distances of $1\text{–}30R_*$. Our extension of HSVK's and LA's analyses to include flared reprocessing disks does not change this conclusion; the observations require both types of disks to be optically thin inside disk radii of $\sim 10\text{–}20R_*$ and thus to emit much less near-infrared radiation than an optically thick disk. We also agree with HSVK's and LA's conclusion that the disk accretion rate must approach $\sim 10^{-5}\ M_\odot\ \mathrm{yr}^{-1}$ to produce significant 3 μm peaks in the spectral energy distribution (top panels in Fig. 3).

Surprisingly, the F-type stars in the sample do not require large mass accretion rates with optically thin inner disk "holes." Figure 4 shows that disks with large $\dot{M}$ and inner holes exceeding $3R_*$ produce unacceptable fits to the observations in Figure 2*c*.

3.2. *Energy Problem*

The disk model for the 3 μm peaks in Ae/Be stars, which requires a large accretion rate and a central "hole" with radius $\sim 5\text{–}20$ stellar radii, raises troubling questions. The total luminosity released by a steady accretion disk with inner radius R_i is $GM\dot{M}/R_i$, so the accretion luminosity generated from $\dot{M} \sim 10^{-6}\text{–}10^{-5}\ M_\odot\ \mathrm{yr}^{-1}$ *exceeds* the luminosity of most Ae/Be stars if this material reaches the stellar surface (see top panels in Fig. 3). Thus, unless the accretion flow actually stops at $R_i = 10R_*$, the observed IR excess emission represents only 10% of the total accretion luminosity. Where is this missing accretion energy emitted? The UV spectra of modestly reddened Ae/Be stars resemble the spectra of normal A-B main-sequence stars (Fig. 2; see also Catala 1989), so these objects show no evidence of missing energy at wavelengths $\sim 0.1\text{–}0.3$ μm. Although interstellar extinction makes it impossible to detect shorter wavelength continuum radiation from these stars, a significant flux below the Lyman limit would produce very intense, optical He I and He II emission lines, EW $\gtrsim$ 10–20 Å (see Kenyon 1986), that are not observed in any Ae/Be star. In addition, the missing luminosity exceeds the apparent stellar luminosity in some cases, and it is not clear how this energy could be "hidden" and leave the stellar photosphere unchanged. As we show in the following subsection, the requirement of large disk accretion luminosities also poses problems in understanding the physical nature of the disk "holes."

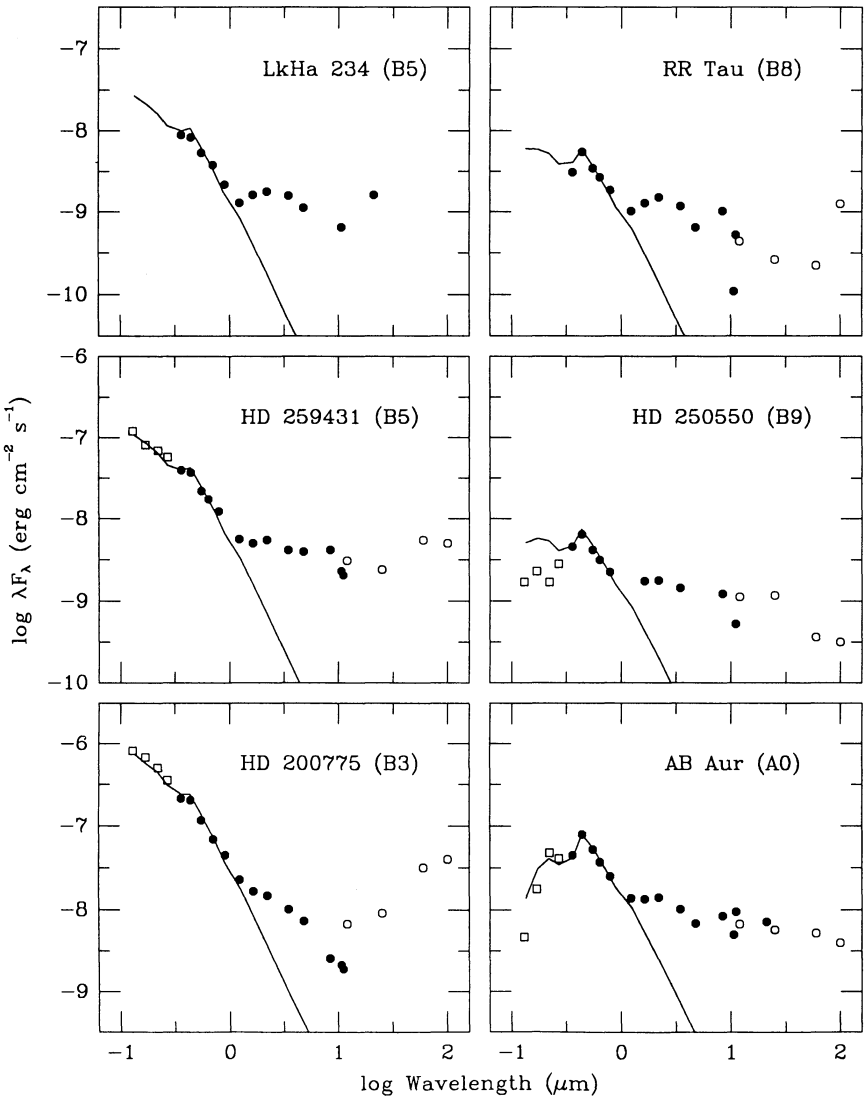

FIG. 2a

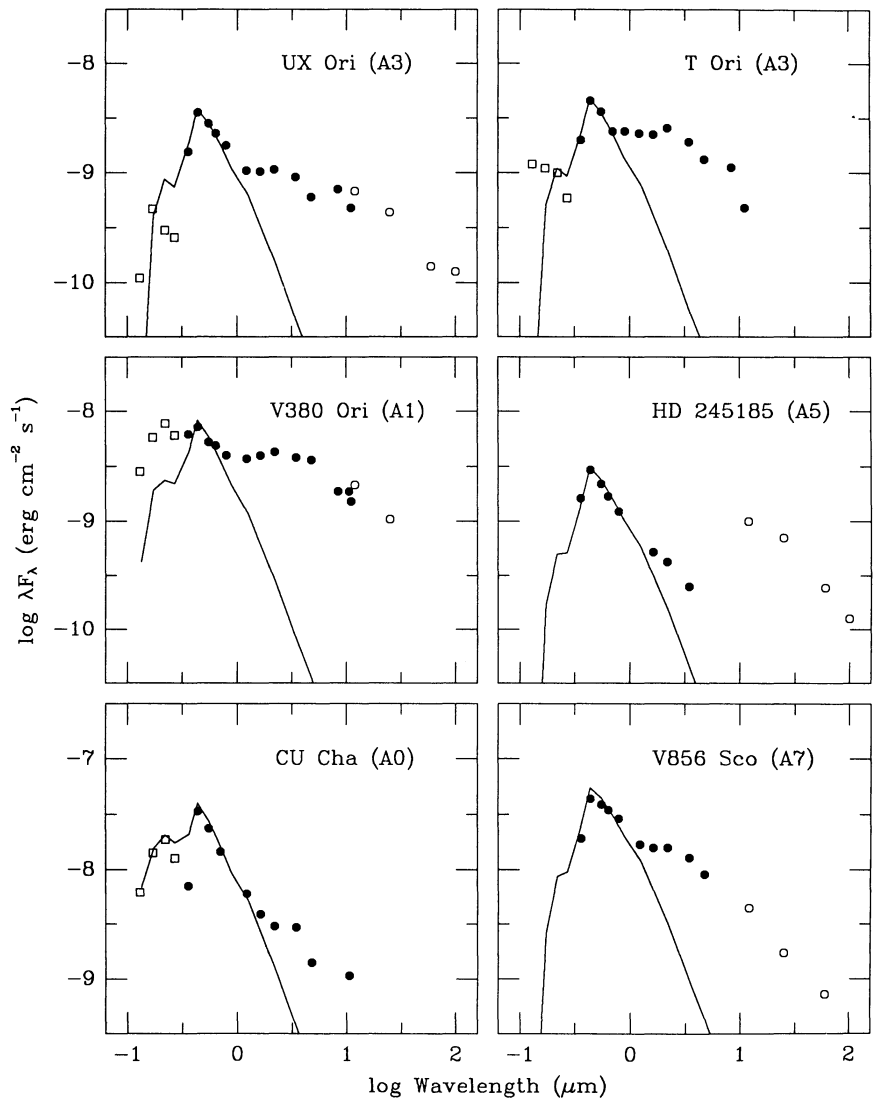

FIG. 2b

FIG. 2.—(*a–c*) Dereddened spectral energy distributions for selected Ae/Be stars derived from published photometry described in the main text. Optical and near-infrared data have been plotted as filled circles, while *IUE* and *IRAS* observations are indicated by boxes and open circles, respectively. The solid line in each panel indicates the energy distribution for a normal main-sequence star chosen to match the spectral type of each Ae/Be star.

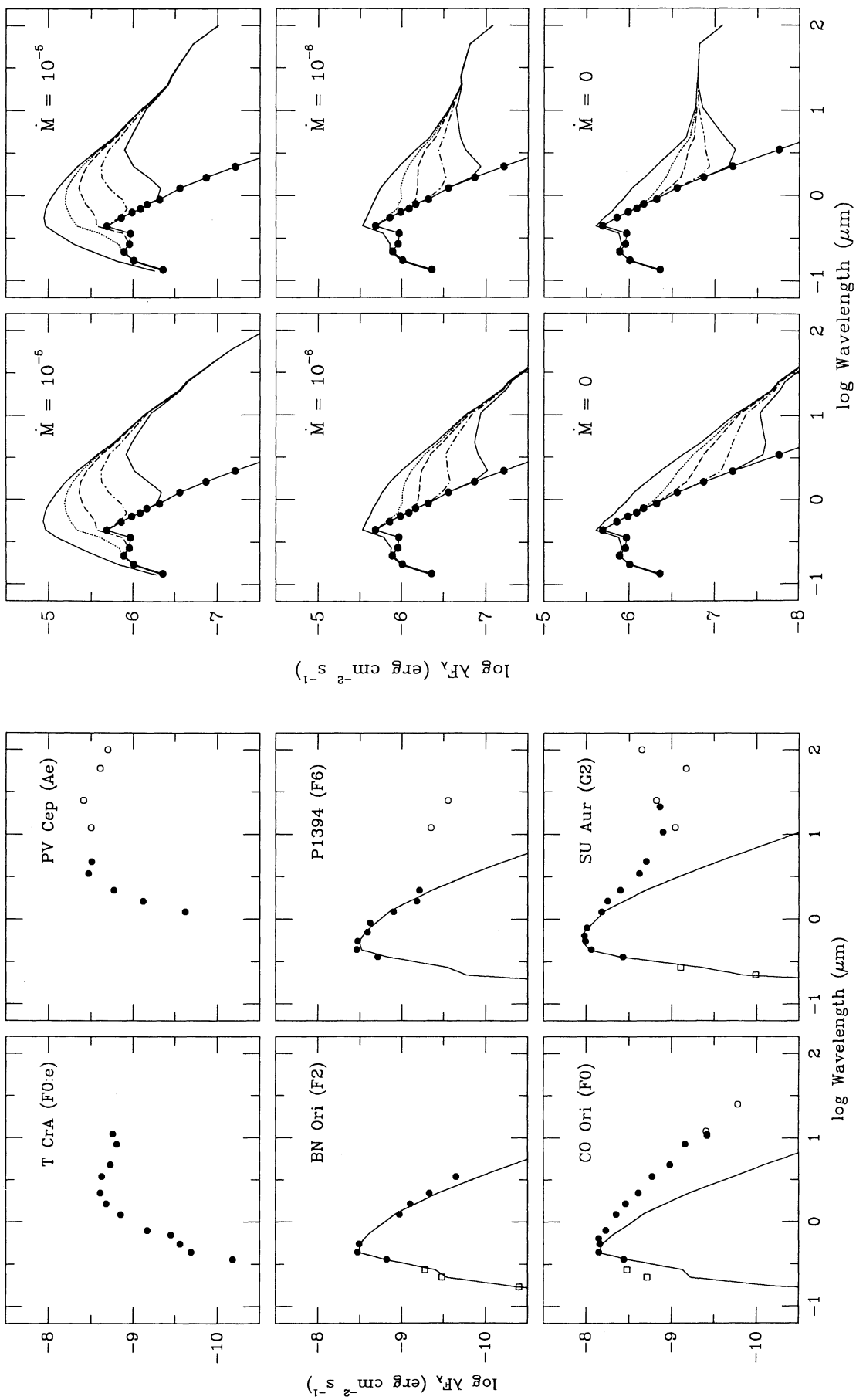

FIG. 2c

FIG. 3.—Simple optically thick blackbody disk models viewed at an inclination of 0° and surrounding a central star having $L = 50\ L_\odot$ and $T_{\rm eff} = 10^4$ K. The left panels show results for flat disks with accretion rates of 0 (*lower left*), 10^{-6} (*middle left*), and 10^{-5} (*upper left*) $M_\odot\ {\rm yr}^{-1}$, while the right panels repeat these accretion rates for flared disks in which the height of the disk photosphere, h, increases with disk radius, R, as $h/R = 0.1(R/R_*)^{1/8}$. In each panel, the filled circles connected by a solid line plot the energy distribution of an A0 main-sequence star; the uppermost solid curve represents the model prediction for an optically thick, blackbody disk extending to the stellar photosphere. The four middle curves plot energy distributions for disk models with inner disk radii of $3R_*$ (*dotted curves*), $5R_*$ (*dashed curves*), $10R_*$ (*dot-dashed curves*), and $20R_*$ (*solid curves*).

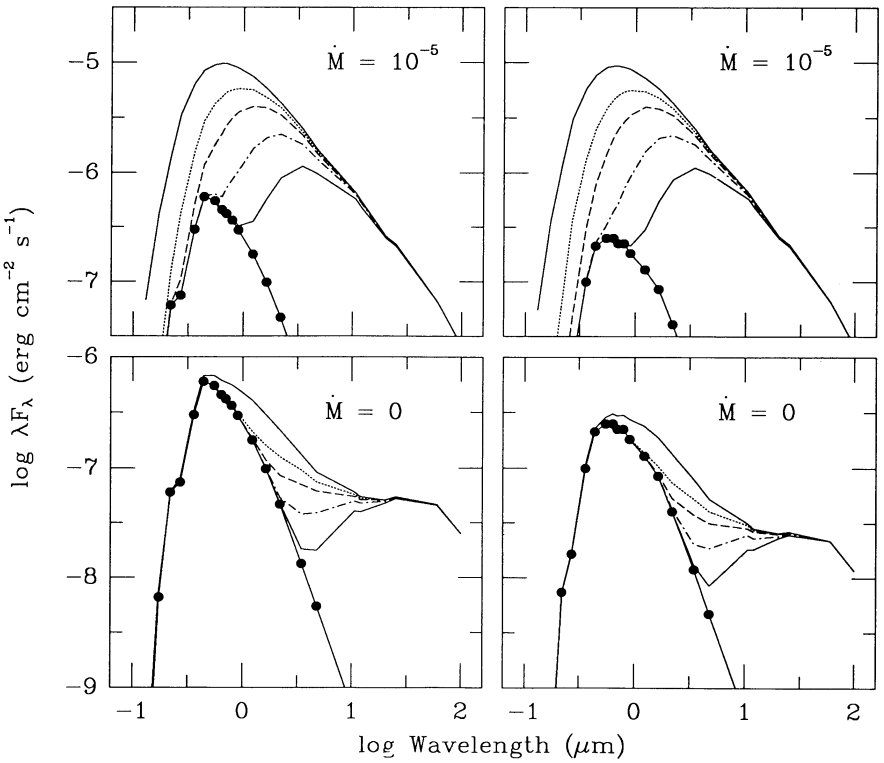

FIG. 4.—Simple optically thick blackbody disk models for central stars of F0 (*left*) and G0 (*right*) spectral types. These plots are for flared disks—as in the right panel of Fig. 3—and have inner holes as described in Fig. 3.

3.3. *Optically Thin Disk Model*

Dust grains dominate the opacity below temperatures of $\sim$2000 K, so both HSVK and LA associated the turnover in disk emission shortward of 3 μm with the lower opacity of gaseous material in which dust grains have been evaporated. However, the temperature of disk material should increase as this gas drifts toward a stellar surface with a temperature of $\sim 10^4$ K; the optical depth must also increase, because the gas opacity increases significantly with increasing temperature. Thus, even if disk material at 10–20R_* is optically thin at a temperature of $\sim$2000 K, hotter disk annuli closer to the central star may become optically thick.

To examine this problem more carefully, we calculated disk optical depths for optically thick and optically thin limits in the standard steady state α-disk approximation (Shakura & Sunyaev 1973). For the optically thick case, we followed Calvet et al.'s (1991) methods for calculating disk model atmospheres to account for the absorption of light from the central star by the disk. These computations ignore viscous dissipation in the disk atmosphere and assume a flared disk geometry, described above, in radiative equilibrium. We divide the disk into concentric annuli and determine the atmospheric structure at each radius for three input parameters: the steady mass flow rate through the disk, $\dot{M}$, and the energy and incidence angle of the stellar radiation. We define the atmosphere as that portion of each annulus where the Rosseland optical depth is ≤ 1. The atmosphere's mass column density is then $m(\tau_{\rm Ross} \sim 1)$, which we adopt as the minimum mass for an optically thick annulus.

Figure 5 shows this minimum mass column density as a function of disk radius (continuous line). The column density to $\tau \sim 1$ varies inversely with opacity, so changes in the minimum mass column density with radius reflect the dependence of the Rosseland mean opacity with temperature. Radiation from the central A0 star and viscous heating keeps disk atmospheric temperatures close to 6000–7000 K for $R \sim R_*$; the opacity then approaches 1 cm^2 g^{-1} due to contributions from H^-. As the disk's effective temperature decreases with increasing radius, the opacity falls by several orders of magnitude when molecules such as H_2O and CO become the dominant opacity source. The opacity increases dramatically when the disk reaches our adopted dust condensation temperature, 1500 K, so the minimum mass column density decreases as the disk approaches $T = 1500$ K at $R \sim 10R_*$. The dust condensation radius slowly increases with increasing $\dot{M}$, because the disk temperature increases as $\dot{M}^{1/4}$.

The total mass column density of a thin, steady accretion disk with mass accretion rate $\dot{M}$ at radius R is given by

$$\Sigma = [(\dot{M}/\alpha c_s H)(1 - (R_*/R)^{1/2}] , \quad (1)$$

(Shakura & Sunyaev 1973; see also Lynden-Bell & Pringle 1974), where c_s is the sound speed, H is the midplane scale height, and the viscosity is $\alpha c_s H$. Both c_s and H depend on $\dot{M}$ and R, so α sets the total mass column density of a particular annulus for an adopted $\dot{M}$.

Figure 5 also shows Σ as a function of radius for $\alpha = 0.1$ (dashed lines) and $\alpha = 10^{-3}$ (dotted lines). The innermost disk annuli become optically thin only for low $\dot{M}$ and high α. Our models suggest the disk is optically thick everywhere unless $\dot{M} < 10^{-6}\ M_\odot$ yr^{-1} and $\alpha \gtrsim 0.1$. Turbulent viscosity disk models require $\alpha \lesssim 1$ (Pringle 1981), which is also consistent with estimates based on models for pre–main-sequence objects (Clarke, Lin, & Pringle 1990; Basri & Bertout 1989). Thus,

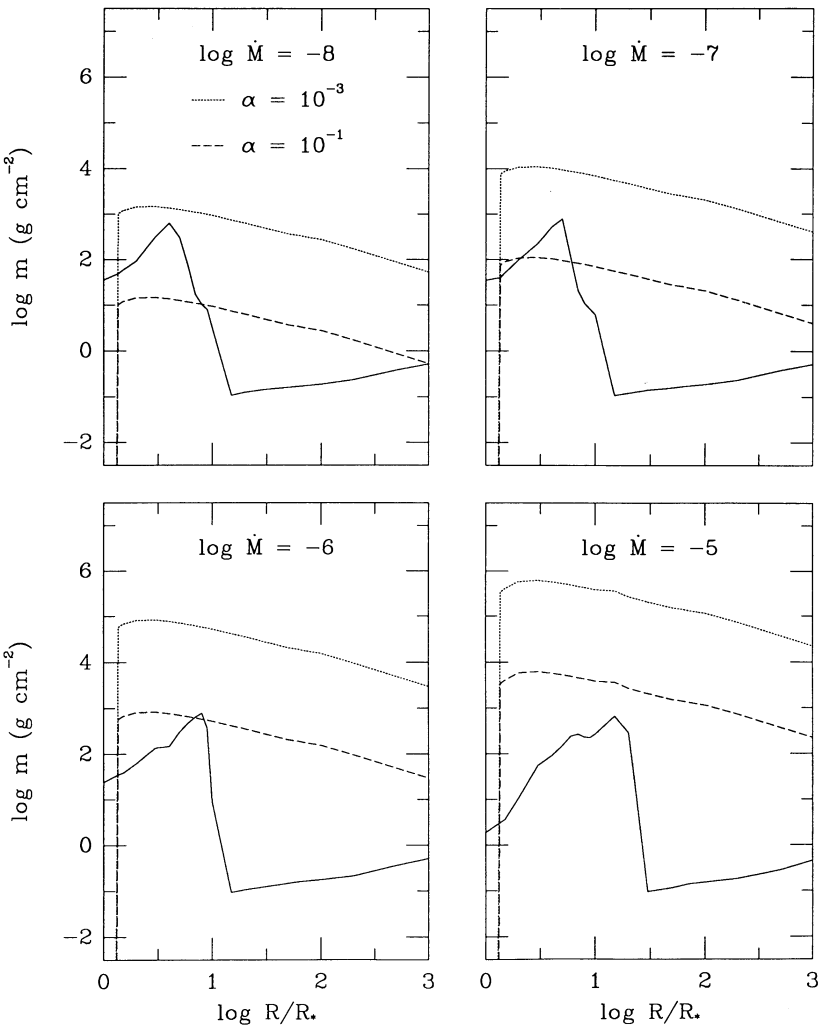

FIG. 5.—Minimum mass column densities required for optically thick irradiated disks, calculated for four different accretion rates (see text). The solid line indicates column densities at which the Rosseland mean optical depth equals unity as a function of radius. The dotted and dashed lines in each panel show the predicted total column density as a function of radius for α disk models for $\alpha = 10^{-3}$ (*dotted lines*) and $\alpha = 10^{-1}$ (*dashed lines*).

based on this analysis, $\dot{M} \lesssim 10^{-6}\ M_\odot\ \mathrm{yr}^{-1}$ seems required to produce an optically thin inner disk.

The optically thick disk calculation ignores viscous dissipation in the atmosphere, which should increase the gas temperature and the optical depth. To verify this, we computed the atmospheric structure for an optically thin, isothermal disk (see Carr 1989; Tylenda 1985). We modified Carr's method by using the E_2 exponentional function to calculate the flux integral and solve the radiative transfer equation. This procedure implicitly evaluates the temperature and accounts for the temperature dependence of both the scale height, H and the opacity. Having obtained a solution *assuming* that the disk is optically thin, we then compute the optical depth through the disk to verify the assumption.

Figure 6 shows the Rosseland mean optical depths through the disk for three different mass accretion rates and $\alpha = 1$. As expected, the inclusion of viscous dissipation raises the atmospheric temperature and thus increases the calculated disk optical depths. The assumption of small optical depth is not valid for the models with accretion rates of 10^{-5} and $10^{-6}\ M_\odot$ yr^{-1}, and therefore disks with accretion rates exceeding 10^{-6} $M_\odot\ \mathrm{yr}^{-1}$ must be optically thick. The $\dot{M} = 10^{-7}\ M_\odot\ \mathrm{yr}^{-1}$ disk is optically thin only between ~ 2–$6R_*$. (In regions where the computed optical depths are $\gtrsim 1$, the calculations are inconsistent and the resulting optical depth curves are incorrect.) Combining results from Figures 5 and 6, we conclude that the disks of Ae/Be stars can be optically thin only if $\dot{M} \lesssim 10^{-7}\ M_\odot\ \mathrm{yr}^{-1}$, assuming $\alpha \leq 1$.

LA suggested that disks with mass accretion rates $\lesssim 10^{-5}$ $M_\odot\ \mathrm{yr}^{-1}$ can be optically thin. Our calculations disagree with this result for two reasons. First, LA assume a radial accretion velocity, v_r, comparable to the sound speed, c_s, whereas the radial velocity in an α disk varies as $v_r \sim (3/2)\alpha c_s(H/R)$ (see, e.g., Pringle 1981). Standard thin disk models have $H/R \sim 0.1$ in the inner disk, so our infall velocities are an order of magnitude smaller than assumed by LA if $\alpha \sim 1$, and thus our disk densities are an order of magnitude higher for the same accretion rate. LA further consider only one disk temperature, $T = 2000$ K, even though much of the inner disk exhibits temperatures well above this estimate. Our models therefore indicate that most of the disk remains optically thick even in regions where dust has been destroyed.

The results suggest the inner annuli of disks surrounding Ae/Be stars remain optically thick unless accretion has no

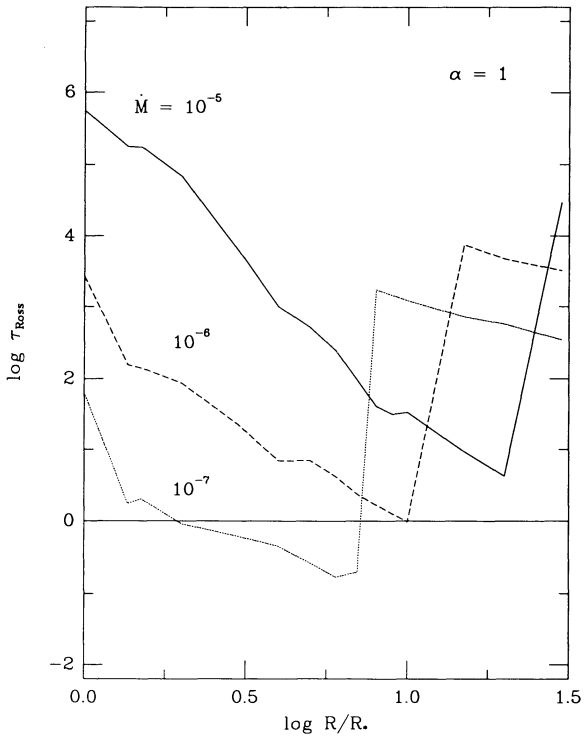

FIG. 6.—The optical depth calculated for disks with $\alpha = 1$ and the indicated mass accretion rates, assuming that the disk is optically thin. The results indicate that the optically thin assumption is valid only for $\dot{M} \lesssim 10^{-7}\ M_\odot\ \mathrm{yr}^{-1}$ in a zone $2 \lesssim R/R_* \lesssim 6$. These calculations suggest disks will be optically thick for even lower mass accretion rates than indicated in Fig. 5; the difference results from viscous dissipation, which heats the optically thin disks to higher temperatures than the photospheres of optically thick disks.

importance on an evolutionary time scale—that is, unless $\dot{M} \lesssim 10^{-7}\ M_\odot\ \mathrm{yr}^{-1}$. Thus, if circumstellar disks must have mass accretion rates exceeding $\sim 10^{-6}\ M_\odot\ \mathrm{yr}^{-1}$ to explain the near-infrared spectral energy distributions of Ae/Be stars (HSVK; LA; § 2.3), there must be real, physical holes in the inner regions of these disks, with radii $R \sim 10R_*$.

Our models further predict no significant difference between the inner regions of disks having comparable $\dot{M}$ surrounding pre–main-sequence A and F stars. We estimate a dust destruction radius of $\sim 5R_*$ for an F0 star with a reprocessing disk and $\dot{M} = 0$. and this radius should increase to $\sim 9R_*$ for high $\dot{M}$. Observations probably could detect a disk with a $5R_*$ inner hole, while a $9R_*$ hole rivals hole sizes envisioned for Ae/Be stars (Fig. 4). However, the data suggest that F-type pre–main-sequence stars have no obvious 3 μm peaks in their spectral energy distributions, which contrasts sharply with the appearance of Ae and Be stars (Fig. 2). In fact, the spectral energy distributions of both F- and G-type pre–main-sequence stars (e.g., SU Aur in Fig. 2*c*) more closely resemble those of the late-type T Tauri stars—which can be fitted with relatively low mass accretion rates $\lesssim 10^{-6}\ M_\odot\ \mathrm{yr}^{-1}$ and small or negligible inner holes $\lesssim 2$–$3R_*$ (Bertout et al. 1988; Hartigan et al. 1991)—than the energy distributions of Ae/Be stars. This behavior suggests a mechanism which produces 3 μm peaks in A and B stars but not in F stars; we consider such a mechanism in § 4.

3.4. *Disk + Magnetosphere Model*

HSVK suggest that the inner disk holes might be physical, not just optically thin regions, and could be caused by a stellar magnetosphere that holds the inner edge of the disk away from the stellar surface (e.g., Königl 1991). This model requires surface magnetic fields of ~ 10 kG (HSVK), which seem rather large but not impossible. The biggest disadvantage of this model is that it predicts a very large accretion luminosity when freely-streaming material strikes the star (§ 3.1), and this accretion luminosity is not apparent in the observations (§ 2.2), nor is this energy likely to be emitted in the unobservable ultraviolet (§ 3.1).

Calvet & Hartmann (1992) and Krautter, Appenzeller, & Jankovics (1990) note that the inverse P Cygni profiles seen in some T Tauri stars provide evidence for magnetosphere accretion. In this model, material falling along magnetic field lines develops sufficiently large radial velocities to explain the observed line widths and velocity shifts. In general, there is little evidence for inverse P Cygni profiles in Ae/Be stars. There is some suggestion of redshifted absorption in R CrA (Graham 1992; Hamann & Persson 1992b, c), but the low luminosity of this system suggests that the central star may really be a rapidly accreting T Tauri variable rather than an A or B star.

Another disadvantage of the magnetosphere model is that there is no obvious reason why the magnetic field should always limit the disk to temperatures $\lesssim 2000$ K when the field can easily couple to the disk at far lower temperatures and fractional ionizations (Königl 1989). One might expect a substantial range in the magnetospheric radius since the accretion rates vary by one to two orders of magnitude among Ae/stars, unless the stellar magnetic fields vary to compensate.

4. ENVELOPE HYPOTHESES

All Herbig Ae/Be stars must possess reflection nebulosity and therefore be surrounded by dusty envelopes (Herbig 1960). A dusty envelope is a particularly attractive way to produce excess infrared emission, because it can cover a larger fraction of the sky (as seen from the central star) than can a thin disk. In principle, a dusty envelope can explain the excesses of Group I sources without *any* accretion energy, which eliminates the "missing luminosity" problem associated with accretion disks (see § 3.2). However, simple radiative equilibrium models require dust grains close to the central star, so the missing luminosity problem remains if envelope material falls onto the central star (§ 4.1). Fortunately, near-infrared emission from embedded companions (§ 4.2) and nonequilibrium radiative processes in small dust grains (§ 4.3) can produce substantial 3 μm emission at large distances from the central star with negligible infall rates. In the following subsections, we examine several variants of the dusty nebula hypothesis and consider their ability to explain the observed near-infrared emission.

4.1. *Infalling Envelopes*

Most theories expect infalling envelopes of molecular gas during the early stages of the star formation process (see Shu, Lizano, & Adams 1987), while models of infall onto luminous pre–main-sequence stars predict inner zones devoid of dust (e.g., Larson 1969; Stahler, Shu, & Taam 1980). Dust evaporation commonly occurs at temperatures of 1000–2000 K, so envelope material just outside the dust destruction region is an attractive location to produce a near-infrared excess.

To examine this possibility, we constructed spherically symmetric radiative equilibrium models of dusty envelopes around Ae/Be stars. Our calculation employs the Unsöld-Lucy method, generalized to spherical symmetry, to derive the radiative equilibrium temperature profile in the envelope and

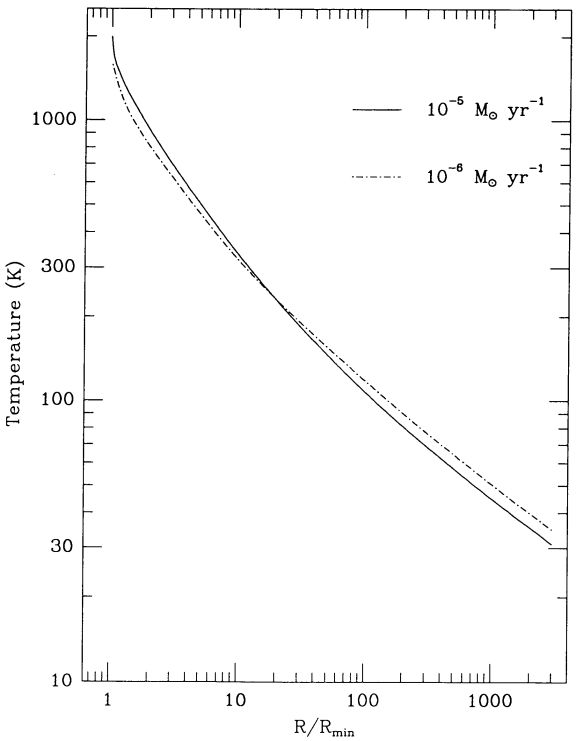

FIG. 7.—The radial temperature distributions for a 10^4 K star surrounded by an infalling dust envelope with two different accretion rates. The horizontal coordinate is radial distance in units of R_{min} = 1 A.U., which is the inner edge of the dust shell in these models.

solves the transfer equation for the mean intensity and flux using variable Eddington factors (Mihalas 1978). These models use values for the dust opacity and albedo from Draine & Lee (1984), as modified by Draine (1987). We assume the envelope density varies with spherical radius as $r^{-1.5}$ and adopt inner and outer envelope radii of 1 AU and 3000 AU, respectively. This choice of inner radius yields maximum envelope temperatures close to the expected point of dust evaporation. For simplicity, we assume the central star radiates as a blackbody with effective temperature of 10,000 K and a radius of 3.45 $R_\odot$ and specifically exclude radiation from a circumstellar disk.

We computed models for two accretion rates—10^{-6} $M_\odot$ yr^{-1} and 10^{-5} $M_\odot$ yr^{-1}—that span plausible infall rates for molecular clouds (Adams et al. 1987). The temperature at the inner edge of the envelope varies with the infall rate. Figure 7 shows that the two model temperature distributions are very similar; the slightly different inner temperature results from our fixed inner radius of 1 AU, but this difference is not important for the discussion that follows.

Figure 8 presents emergent fluxes for these spherically symmetric envelope calculations. The 10^{-6} $M_\odot$ yr^{-1} model shows the 3 μm near-infrared peak required by observations. Some systems (e.g., AB Aur) also display the predicted 10 μm silicate emission feature, while other objects (such as MWC 1080) have featureless 10 μm spectra (Cohen 1980). The 10^{-5} $M_\odot$ yr^{-1} model fails to agree with observations; it produces too little near-infrared emission, because the extinction through the envelope is too large. In both models, the optical extinction to the central star far exceeds that estimated from the observations (HSVK).

These optically thick envelope models can be reconciled with observations of most Ae/Be stars only if there is a clear

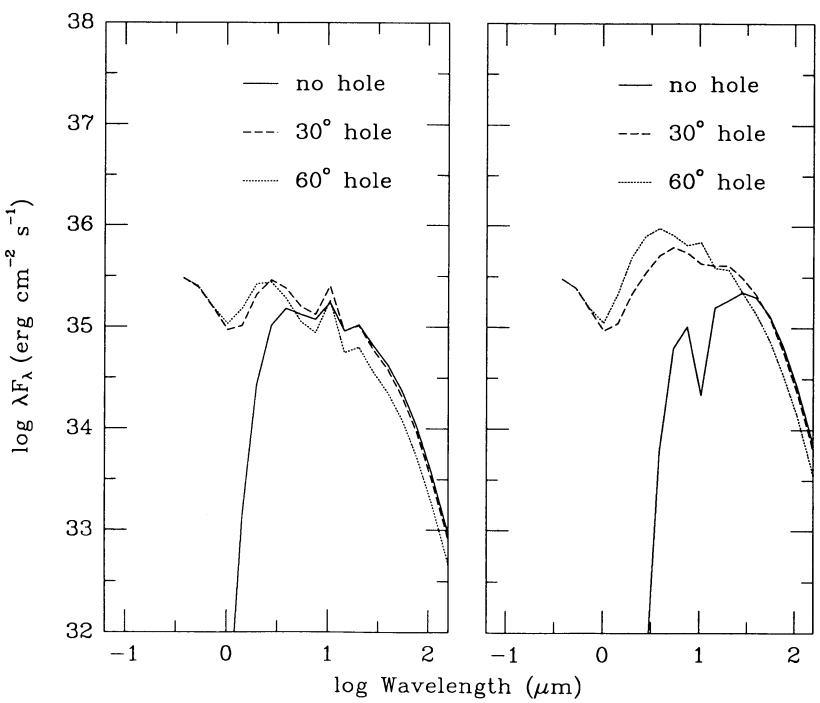

FIG. 8.—Spectral energy distributions for dust envelope models surrounding a 10,000 K central star and the radial temperature distributions displayed in Fig. 7. The envelope material falls at the indicated mass accretion rates, as described in the text. The solid lines show spectra calculated for spherically symmetric envelopes, while the other lines present results for envelopes with conical holes along the line of sight to the star. The holes subtend angles from the polar axis of 30° (*dashed lines*) and 60° (*dotted lines*). *Left*: 10^{-6} $M_\odot$ yr^{-1}. *Right*: 10^{-5} $M_\odot$ yr^{-1}.

line of sight to the central star. The bipolar outflows associated with many of the youngest stars naturally create large cavities in the collapsing cloud (see Lada 1985; Edwards, Mundt, & Ray 1992), so an observer viewing the system down the outflow has a fairly clear view of the central star. This geometry guarantees the observer a good line of sight to the hot inner regions of the envelope that produce the near-infrared peak in the spectral energy distribution. In effect, this infalling model envelope with cavities is roughly equivalent to a "thick disk" with a dust destruction zone. Kenyon & Hartmann (1991) recently applied a similar model to the FU Orionis variable V1057 Cyg, which can account for the observed 10–100 μm excess with modest extinction toward the central star and inner accretion disk.

A complete calculation for the spectral energy distribution of an envelope with a bipolar cavity requires a time consuming radiative transfer solution in three dimensions. Instead, we employ an approximate method that retains the essential features of the problem. We adopt the temperature distribution from the spherically symmetric calculation and assume that the envelope has a conical hole with a fixed opening angle from the axis of symmetry. We then calculate the emergent spectrum for an observer viewing the system pole-on (see Kenyon & Hartmann 1991). This procedure overestimates the temperature—and hence the near-infrared emission—of the inner envelope, because a spherical envelope traps stellar radiation that would escape out of a bipolar cavity. Given the uncertainty in the exact temperature of dust sublimation, this simple model should be adequate to illustrate the basic situation.

Figure 8 shows spectral energy distributions for two basic envelope models assuming conical holes of 30° and 60° from the line of sight. These results agree reasonably well with observations: the infrared excess peaks at 2–3 μm and the spectral slope from 3.5 μm to 10 μm follows d log F_ν/d log $\nu = -0.05$ to 0.32 (HSVK). However, most of the observed spectral energy distributions (HSVK; Fig. 2) do not show evidence for the strong silicate emission peak shown by our low accretion rate model and are more consistent with the 10^{-5} $M_\odot$ yr^{-1} model. Accretion rates higher than 10^{-6} $M_\odot$ yr^{-1} may be required to accrete sufficient mass during the pre–main-sequence time scale of $\lesssim 10^6$ yr predicted by standard evolutionary tracks for stars more massive than 3 $M_\odot$ (see Cohen & Kuhi 1979).

The infalling envelope model demands that we view a significant fraction of Ae/Be stars through their dusty envelopes and not along an evacuated cavity or hole. HSVK's sample included 11 Group II sources compared with 30 Group I sources, which suggests that envelopes covering $\sim 25\%$ of solid angle are consistent with the observations. The covering factor could be larger than 25% if we are biased against detecting heavily extincted sources, which seems likely.

The infalling envelope can emit large amounts of near-infrared radiation without requiring direct dissipation of accretion energy. However, this envelope model possesses essentially the same luminosity problem as the disk models, because the infall rates are similar. The luminosity problem can be delayed if envelope material has sufficient angular momentum to avoid falling directly onto the star and instead falls at much larger radii onto a circumstellar disk (Cassen & Moosman 1981; Terebey, Shu, & Cassen 1984). We feel this solution requires too much fine tuning to be generally applicable to Ae/Be stars. If the dusty material has too much angular momentum, it falls at large disk radii and never gets hot enough to emit near-infrared radiation; if the material has too little angular momentum, then it falls too close to (and obscures) the central star. Even if material does generally fall onto the disk at 1 AU, the disk either accretes this material onto the central star and produces an unacceptably large accretion luminosity or stores the material, grows to an unstable mass on short time scale ($\lesssim 10^5$ yr), and rapidly accretes material onto the central star.

To summarize, we find that infalling envelopes with plausible accretion rates can explain the near-infrared emission of some Ae/Be stars if bipolar flows evacuate cavities along which the central star and inner envelope can be observed. That several Ae/Be stars are heavily extincted adds some support to this interpretation (see also Berrilli et al. 1992). On the other hand, this model requires a limited range of envelope parameters to explain observations. In particular, the model requires infall to distances of ~ 1 AU without concurrent disk accretion onto the central star at similar rates. The restrictive nature of these assumptions suggests that infalling envelopes cannot account for the infrared excesses of most Ae/Be stars.

4.2. *Companion + Envelope Hypothesis*

Recent observations have revealed several infrared companions to optically visible T Tauri stars (e.g., Dyck, Simon, & Zuckerman 1982; Leinert & Haas 1989; Haas, Leinert, & Zinnecker 1990). The spectral energy distributions for some of these companions—such as T Tau, XZ Tau, and GV Tau (Haro 6-10)—resemble energy distributions of the youngest, most heavily embedded young stars in molecular clouds (see, for example, Leinert & Haas 1989) and presumably emit most of their radiation at near-infrared or far-infrared wavelengths because they are surrounded by opaque, dusty envelopes (e.g., Adams et al. 1987; Myers et al. 1987). Several Ae/Be stars—such as XY Per (Herbig & Bell 1988)—possess optical companions at distances of several arcseconds, so other Ae/Be stars with more opaque reflection nebulosities might have embedded companions visible only at near-infrared wavelengths.

Figure 9 shows the potential for explaining the 3 μm peaks of Ae/Be stars with an embedded companion. This figure plots the sum of fluxes from a typical A star and the embedded companion to T Tau (Ghez et al. 1991). The results resemble observations of several Ae/Be stars, such as LkHα 234 and RR Tau (Fig. 2). Although Figure 9 suggests that embedded companions might account for several of the observed energy distributions, we agree with HSVK that embedded companions seem an unlikely solution to the general phenomenon of 3 μm excesses. As we explained in § 2, 17 out of 24 Group I objects display 3 μm peaks in their spectral energy distributions. If roughly half of main-sequence A & B stars are binaries (Abt 1983), then *all* Ae/Be stars would need a companion embedded in an envelope with $A_V \sim 10$ mag to explain the frequency of observed 3 μm peaks. In reality, we expect a range in envelope extinctions from roughly zero (as in the XY Per binary) to $\gg 10$ (as in a typical embedded protostar), so we might anticipate 2–3 near-infrared companions in a sample of 24 objects.

4.3. *Transiently Heated (Small) Grain Hypothesis*

As noted in § 2.2, medium-resolution near-infrared spectra of Ae/Be stars such as CU Cha, Elias 1, TY CrA, XY Per, and HD 245185 show evidence of emission features also seen in reflection nebulae near hot stars (Whittet et al. 1983; Brooke & Tokunaga 1992). These observations constitute direct evidence

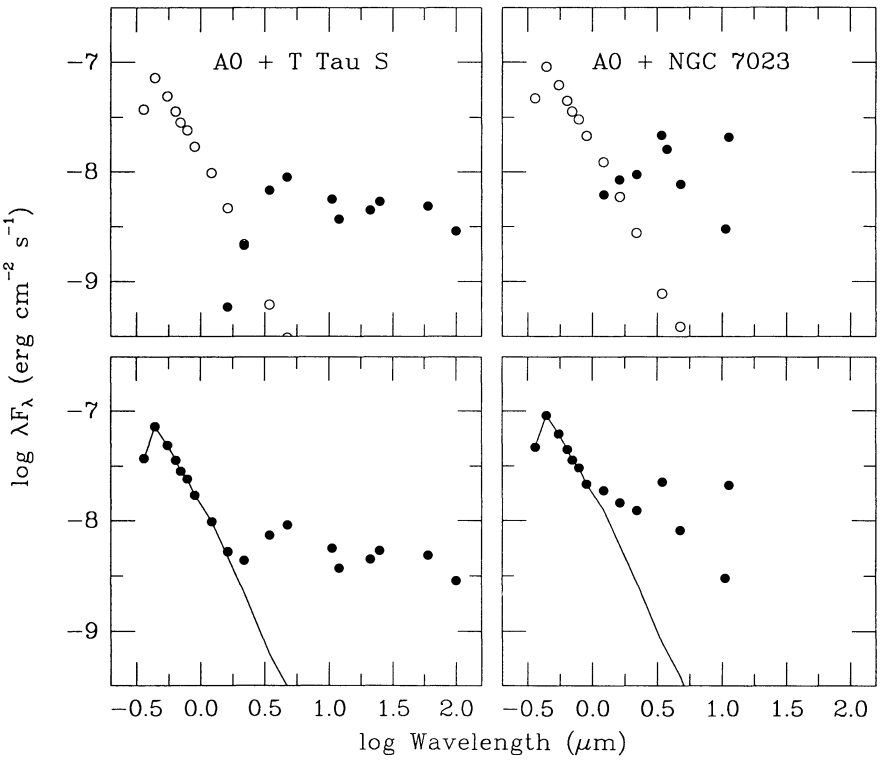

FIG. 9.—*Top, bottom left*: Spectral energy distributions of an A0 star and the infrared companion of T Tauri (Ghez et al. 1991), plotted separately (*top left*) and added together (*bottom left*) to illustrate the combined spectrum of an Ae/Be star and an infrared companion. *Top, bottom right*: Broad-band colors of the reflection nebula of NGC 7023 at a position 30″ W and 20″ north of the Ae/Be star HD 200775, taken from the measurements of Sellgren (1984) and Sellgren et al. (1985). The upper right panel shows the spectral energy distribution of the nebula relative to an A0 star, the bottom right panel shows the sum of the two arbitrarily scaled (see text).

that a mechanism (or mechanisms) other than blackbody disk emission contributes to the near-infrared spectrum of at least these objects. We therefore consider whether processes similar to those observed in reflection nebulae can produce the 3 μm peaks seen in other Ae/Be stars.

Sellgren (1984) and Sellgren et al. (1985) have extensively studied the reflection nebula NGC 7023, which surrounds a cluster of pre–main-sequence stars dominated by the Herbig Be star HD 200775. They found a strong near-infrared continuum with an approximate color temperature of 1000 K and 3.3–3.6 μm emission features at angular distances of $\gtrsim 30''$ from HD 200775, which corresponds to a linear distance of nearly 0.1 pc. This infrared emission closely follows the optical scattered light distribution and totals ~1% of the stellar luminosity. A thermal equilibrium model cannot explain the presence of 1000 K grains at such large distances from the central star given the luminosity of HD 200775 ($\sim 10^4\ L_\odot$; HSVK). Instead, Sellgren (1984) suggested that transient heating of small grains by ~10 eV photons causes this high-temperature emission (see also Leger & Puget 1984; Allamandola, Tielens, & Barker 1985, 1989; Puget & Leger 1989).

Figure 9 plots the broadband colors of NGC 7023 using surface brightnesses given by Sellgren (1984) and Sellgren et al. (1984), along with a standard A0 star. (The nebula has nearly uniform surface brightness in apertures of 5″–30″). The underlying 1000 K continuum and the very large 3.3–3.6 μm emission feature are quite prominent. There are additional emission features, including one at 11.3 μm. The continuum emission compares favorably with the spectral energy distributions of several Ae/Be stars (Fig. 2). Figure 10 shows this for the near-infrared region by comparing the $J-H$, $H-K$ colors of Ae/Be stars (open circles) with Sellgren's (1984) colors for various positions in NGC 7023 (outlined area). Sellgren noted that the near-IR colors for NGC 7023 did not vary significantly with

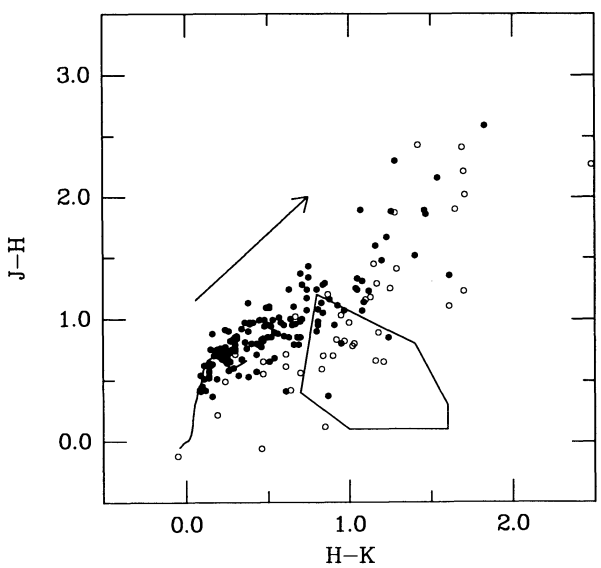

FIG. 10.—$J-H$ vs. $H-K$ colors of T Tauri stars (*filled circles*) and Ae/Be stars (*open circles*), compared with the range of colors observed by Sellgren et al. (1984) in reflection nebulae. The arrow indicates the reddening vector for $A_V = 10$ mag.

position across the nebula and found similar colors for the reflection nebulae NGC 2023 and NGC 2068 (see also Sellgren, Werner, & Dinerstein 1983). Figure 10 clearly demonstrates that nebular emission—modified appropriately for different reddenings—can explain the near-infrared colors of the majority of Ae/Be stars.

However, the 3.3–3.6 μm emission features in NGC 7023 produce a larger peak than observed in some Ae/Be stars, which would require the relative strength of the 3.3–3.6 μm features generally be reduced or suppressed. It is difficult to prove that this can be accomplished, because the physical mechanisms responsible for emission features at 3.3–3.6, 6.2, 7.7, 8.6, and 11.3 μm (possibly PAH molecules; see Puget & Leger 1989), not to mention the near-infrared continuum, are not very well understood. The emission features vary substantially among the Ae/Be stars in which they have been detected (Whittet et al. 1983; Brooke & Tokunaga 1992). It appears possible the molecules responsible for the emission features might be destroyed close to the hot central star (although there may need to be an absence of dust close to the star to suppress the 3.43 and 3.53 μm features; Schutte et al. 1990).

The geometry and physical properties of the required dusty envelope are difficult to predict or constrain given the uncertainties in emissivities, dust properties, etc. (Allamandola et al. 1989; Guhathakurta & Draine 1989). Observationally, the excesses are observed with typical apertures of 5″–10″, corresponding to typical projected size scales of several thousand A.U. As pointed out above, Sellgren (1984) found that the near-infrared emission of NGC 7023 is $\sim 1\%$ of the total luminosity of HD 200775. For some Ae/Be stars, the required near-infrared luminosities are of the order of a few percent (e.g., LkHa 234, HD 259431, HD 200775, HD 245185, CU Cha; Fig. 2), suggesting that the required efficiency of conversion from ultraviolet to near-infrared emission is consistent with the reflection nebula hypothesis. On the other hand, some objects have much larger near-infrared excess emission, of order tens of percent of the total (e.g., RR Tau, HD 250550, AB Aur, UX Ori, T Ori, V380 Ori), and this may require unreasonably large conversion efficiencies (i.e., most of the light from the central star would have to be absorbed by small grains). Objects with large excesses may be more reasonably explained by infrared companions.

The presence of 3.3–3.6 μm features in several Ae/Be stars suggests that the dusty nebula hypothesis deserves further consideration, especially for objects whose membership in the Ae/Be class requires the presence of a reflection nebula. Moreover, it offers a solution to the energy problem discussed above. As long as the nebula subtends a reasonably large fraction of solid angle, it can account for the magnitude of the infrared excess. If the nebula is sufficiently distant from the star, there is no reason to suppose it is falling into a disk, and the issue of missing large accretion energies does not arise.

Observational tests of this picture can be made. Other Ae/Be stars should display extended near-infrared (2–4 μm) emission that follows the optical scattered light distribution and emits substantially more radiation than predicted by simple thermal equilibrium models. The nearest Ae/Be stars may exhibit spatially-resolved nebular emission in the near-infrared, which would not be expected in the disk model with its thermal emission confined to distances $\sim 10R_*$. Finally, 3.3–3.6 μm bands should only be observed in stars with sufficiently strong ultraviolet radiation. We showed in § 2 that several pre–main-sequence F stars with infrared excess emission do not show any evidence of 3 μm peaks in their spectral energy distributions; high-resolution spectroscopic observations of these and other F- and G-type pre–main-sequence stars should *not* display 3.3–3.6 μm bands if our model is correct.

4.4. *Disks, Emission Activity, and Evolution*

We have argued that the infrared excess emission of many Ae/Be stars arises primarily from a surrounding dusty envelope (or from an envelope surrounding a companion) rather than from a disk. This does not rule out the presence of modest- to low-accretion rate disks around Ae/Be stars, which would have lower infrared emission than the nebulae. It may be necessary to have such accretion to power the emission-line activity and mass loss, as has been argued for T Tauri stars by Cabrit et al. (1990). Catala, Kunasz, & Praderie (1984), and Catala & Kunasz (1987) derived a mass-loss rate for AB Aur of $\sim 10^{-8}\ M_\odot\ \mathrm{yr}^{-1}$, which is typical of values derived for T Tauri stars (Edwards et al. 1987) with disk accretion rates typically $\sim 10^{-7}\ M_\odot\ \mathrm{yr}^{-1}$ (Hartmann & Kenyon 1990).

On the other hand, the excess line emission is generally a much smaller fraction of the stellar luminosity for Ae/Be stars than it is for T Tauri stars, making it more difficult to rule out direct stellar activity. Some Be stars show emission-line activity without apparently requiring pre–main-sequence disk accretion. Finally, Finkenzeller (1985) found no evidence for systematic blueshifted [O I] emission, as observed for T Tauri stars and interpreted as evidence for disk occultation (Edwards et al. 1987).

The absence of high-accretion rate disks around Ae stars does not imply that they could not have formed from disks. Many of these objects have ages ~ 1–3×10^6 yr (HSVK), and it is conceivable that their disks evolve somewhat faster than the $3 \times 10^6 - 10^7$ yr evolutionary times estimated for T Tauri disks (Strom et al. 1990). In support of this picture, standard evolutionary tracks predict that the T Tau primary will evolve into an early A star, given its spectral type and estimated luminosity (Ghez et al. 1990). Note that the *current* accretion rate for the T Tauri primary is estimated to be $\sim 10^{-7}\ M_\odot\ \mathrm{yr}^{-1}$ (Kenyon & Hartmann 1987), well below the estimates of HSVK and LA for Ae/Be stars.

5. CONCLUSIONS

We have evaluated several circumstellar disk and envelope models developed to explain the infrared excesses of the pre–main-sequence Ae/Be stars. Despite uncertainties concerning spectral types and system luminosities, we draw several general conclusions.

1. By analogy with the low-mass T Tauri stars, circumstellar disks are an attractive way to produce infrared excesses in the intermediate-mass Ae/Be stars. We agree with HSVK and LA that this model is viable only for high accretion rates—$\dot{M} \sim 10^{-6}$–$10^{-5}\ M_\odot\ \mathrm{yr}^{-1}$—and disks with inner holes—$R_i \sim 10$–$20R_*$. However, our results suggest that disks surrounding massive young stars remain optically thick at high accretion rates; small optically thin regions occur for the lowest accretion rates ($\lesssim 10^{-7}\ M_\odot\ \mathrm{yr}^{-1}$), and these produce spectral energy distributions that disagree with observations. Thus, we conclude that circumstellar disks are unlikely to be responsible for the observed infrared excesses of most Ae/Be stars.

2. Dusty nebulae offer an appealing alternative to circumstellar disks. One model involves small grains at large distances from the central star. Ultraviolet photons heat these grains to

temperatures of ~1000 K, and the grains then emit near-infrared continuum and line emission as they cool to their equilibrium temperatures of 10–50 K. Observations of the 3.3–3.6 μm emission bands in several Ae/Be stars lend some support to this idea. This model explains the absence of 3 μm peaks in the spectral energy distributions of late-type pre–main-sequence stars, because these stars do not emit enough $h\nu \sim 10$ eV photons to heat a sufficiently large population of small dust grains to 1000 K.

3. Embedded companions may provide an additional source of 3 μm emission in some Ae/Be stars. The companion could be embedded in its own envelope or an envelope surrounding the Ae/Be primary star; in either case, this explanation requires a relatively clear line of sight to the primary star and an extinction to the companion of $A_V \sim 10$ mag. Significantly less opaque envelopes produce optical binaries, while more opaque nebulae obscure the companion completely.

4. Our preferred models can be tested by observations. If small dust grains transiently heated to ~1000 K produce the 3 μm excesses, then A- and B-type pre–main-sequence stars should exhibit extended 3 μm emission similar to that observed in the reflection nebula NGC 7023, while F- and later-type pre–main-sequence stars should not be extended. High-resolution near-infrared images could verify if any Ae/Be stars have nearby infrared companions.

We acknowledge Kris Sellgren for extensive and careful comments as referee. We thank Charlie Lada and Steve Strom for useful conversations and comments, Bill Herbst for providing a machine-readable version of his Ae/Be star photometry, Rob Hewett for assisting with the compilation of the near-infrared photometry, and Dan Zucker for obtaining and reducing the *IUE* data. We also acknowledge the NSSDC for providing machine readable versions of The Catalog of Infrared Observations and for providing *IUE* data. This research was supported in part by NASA grant NAGW-2919 and by the International Exchange Program of the Smithsonian Institution.

REFERENCES

Abt, H. A. 1983, ARA&A, 21, 343
Adams, F. C., Lada, C. J., & Shu, F. H. 1987, ApJ, 312, 788
Allamandola, L. J. Tielens, A. G. G. M., & Barker, J. R. 1985, ApJ, 290, L25
———. 1989, ApJS, 71, 733
Basri, G., & Bertout, C. 1989, ApJ, 341, 340
Berrilli, F., Corciulo, G., Ingrotto, G., Lorenzetti, D., Nioni, B., & Strafella, F. 1992, ApJ, 398, 254
Bertout, C., Basri, G., & Bouvier, J. 1988, ApJ, 330, 350
Bessell, M. S., & Brett, J. M. 1988, PASP, 100, 1134
Brooke, T. Y., & Tokunaga, A. T. 1992, BAAS, 24, 798
Cabrit, S., Edwards, S., Strom, S. E., & Strom, K. M. 1990, ApJ, 354, 687
Calvet, N., & Hartmann, L. 1992, ApJ, 386, 239
Calvet, N., Patiño, A., Magris, C. G., & D'Alessio, P. 1991, ApJ, 380, 617
Carr, J. 1989, ApJ, 345, 522
Cassen, P., & Moosman, A. 1981, Icarus, 48, 353
Catala, C. 1989, in Proc. ESO Conf. 33, Low-Mass Star Formation and Pre–Main-Sequence Objects, ed. B. Reipurth (Garching: ESO), 471
Catala, C., & Kunasz, P. B. 1987, A&AS, 174, 158
Catala, C., Kunasz, P. B., & Praderie, F. 1984, A&AS, 134, 402
Clarke C. J., Lin, D. N. C., & Pringle, J. E. 1990, MNRAS, 242, 439
Cohen, M. 1980, MNRAS, 191, 499
Cohen, M., & Kuhi, L. V. 1979, ApJS, 41, 743
Draine, B. 1987, Princeton Obs. preprint, No. 213
Draine, B., & Lee, H. M. 1984, ApJ, 285, 89
Dyck, H. M., Simon, T., & Zuckerman, B. 1982, ApJ, 255, L103
Edwards, S., Cabrit, S., Strom, S. E., Heyer, I., Strom, K. M., & Anderson, E. 1987, ApJ, 321, 473
Edwards, S., Ray, T. P., & Mundt, R. 1992, in Protostars and Planets III, ed. E. H. Levy & M. S. Mathews, in press
Finkenzeller, U. 1985, A&AS, 151, 340
Finkenzeller, U., & Jankovics, I. 1984, A&AS, 57, 285
Finkenzeller, U., & Mundt, R. 1984, A&AS, 55, 109
Gezari, D. Y., Schmitz, M., & Mead, J. M. 1987, Catalog of Infrared Observations, NASA Ref. Publ. 1196
Ghez, A., Neugebauer, G., Gorham, P. W., Haniff, C. A., Kulkarni, S. R., Matthews, K., Koresko, C., & Beckwith, S. 1991, AJ, 102, 2066
Graham, J. A. 1992, PASP, 104, 479
Guhathakurta, P., & Draine, B. T. 1989, ApJ, 345, 230
Haas, M., Leinert, Ch., & Zinnecker, H. 1990, A&A, 230, L1
Hamann, F., & Persson, S. E. 1992a, ApJ, 394, 628
———. 1992b, ApJS, 82, 247
———. 1992c, ApJS, 82, 285
Harris, A. W., & Sonneborn, G. 1987, in Exploring the Universe with the *IUE* Satellite, ed. Y. Kondo (Dordrecht: Reidel), 729
Hartigan, P., Hartmann, L., Kenyon, S. J., Hewett, R., & Stauffer, J. R. 1989, ApJS, 70, 899
Hartigan, P., Hartmann, L., Kenyon, S. J., Strom, S. E., & Skrutskie, M. F. 1990, ApJ, 354, L25
Hartigan, P., Kenyon, S. J., Hartmann, L., Strom, S. E., Edwards, S., Welty, A. D., & Stauffer, J. R. 1991, ApJ, 382, 617
Hartmann, L., & Kenyon, S. J. 1990, ApJ, 349, 190
Herbig, G. S. 1960, ApJS, 4, 337
Herbig, G. H., & Bell, K. R. 1988, Lick Obs. Bull., No. 1111
Herbst, W., Holtzman, J. A., & Klasky, R. S. 1983, AJ, 88, 1648
Herbst, W., Holtzman, J. A., & Phelps, B. E. 1982, AJ, 87, 1710
Hillenbrand, L. A., Strom, S. E., Vrba, F. J., & Keene, J. 1992, ApJ, 397, 613
Kenyon, S. J. 1986, The Symbiotic Stars (Cambridge Univ. Press)
Kenyon, S. J., & Hartmann, L. 1987, ApJ, 323, 714
———. 1990, ApJ, 349, 197
———. 1991, ApJ, 383, 664
Königl, A. 1991, ApJ, 370, L39
Krautter, J., Appenzeller, I., & Jankovics, I. 1990, A&A, 236, 416
Lada, C. J. 1985, ARA&A, 23, 267
Lada, C. J., & Adams, F. C. 1992, ApJ, 393, 278
Larson, R. B. 1969, MNRAS, 145, 271
Leger, A., & Puget, J. L. 1984, A&A, 137, L5
Leinert, Ch., & Haas, M. 1989, ApJ, 342, L39
Lynden-Bell, D., & Pringle, J. E. 1974, MNRAS, 168, 603
Mathis, J. S. 1990, ARA&A, 28, 37
Mihalas, D. 1978, Stellar Atmospheres (San Francisco: Freeman)
Myers, P. C., Fuller, G. A., Mathieu, R. D., Beichman, C. A., Benson, P. J., & Schild, R. E. 1987, ApJ, 319, 340
Pringle, J. E. 1981, ARA&A, 19, 137
Puget, J. L., & Leger, A. 1989, ARA&A, 27, 161
Savage, B. D., & Mathis, J. S. 1979, ARA&A, 17, 73
Schutte, W. A., Tielens, A. G. G. M., Allamandola, L. J., Cohen, M., & Wooden, D. H. 1990, ApJ 360, 577
Sellgren, K. 1984, ApJ, 277, 623
Sellgren, K., Allamandola, L. J., Bregman, J. D., Werner, M. W., & Wooden, D. H. 1985, ApJ, 299, 416
Sellgren, K., Werner, M. W., & Dinerstein, H. L. 1983, ApJ, 271, L13
Shakura, N. I., & Sunyaev, R. A. 1973, A&A, 24, 337
Shu, F. H., Adams, F. C., & Lizano, S. 1987, ARA&A, 25, 23
Sinton, W. M., & Tittemore, W. C. 1984, AJ, 89, 1366
Stahler, S. W., Shu, F. H., & Taam, R. E. 1980, ApJ, 241, 637
Strom, S. E., Edwards, S., & Skrutskie, M. 1990, in Cool Stars, Stellar Systems, and the Sun, ed. G. Wallerstein, ASP Conf. Ser. (San Francisco: ASP) 275
Strom, S. E., Strom, K. M., Yost, J., Carrasco, L., & Grasdalen, G. 1972, ApJ, 173, 353
Terebey, S., Shu, F. H., & Cassen, P. 1984, ApJ, 286, 529
Tylenda, R. 1985, ApJ, 345, 522
Whittet, D. C. B., Williams, P. M., Bode, M. F., Davies, J. K., & Zealey, W. J. 1983, A&A, 123, 301